International Journal of Solids and Structures 49 (2012) 3627–3640

Contents lists available at SciVerse ScienceDirect

International Journal of Solids and Structures

journal homepage: www.elsevier.com/locate/ijsolstr

# Stress analysis of transversely isotropic sectors weakened by multiple defects

R.T. Faal [a,*], A.R. Hassani [a], A.S. Milani [b]

[a] Faculty of Engineering, University of Zanjan, P. O. Box 45195-313, Zanjan, Iran
[b] School of Engineering, University of British Columbia, Kelowna, Canada

ARTICLE INFO

*Article history:*
Received 30 August 2011
Received in revised form 16 July 2012
Available online 9 August 2012

*Keywords:*
Anti-plane
Sector
Transversely isotropic
Stress intensity factor
Hoop stress

ABSTRACT

In this article, the anti-plane deformation of a transversely isotropic sector with multiple defects is studied analytically. The solution of a Volterra-type screw dislocation problem in a sector is first obtained by means of a finite Fourier cosine transform. The closed form solution is then derived for displacement and stress fields over the sector domain. Next, the distributed dislocation method is employed to obtain integral equations of the sector with cracks and cavities under an anti-plane traction. The ensuing integral equations are of the Cauchy type singular and have been solved numerically. A set of examples are presented to demonstrate the applicability of the proposed solution procedure. The geometric and force singularities of stress fields in the sector are also studied and compared to the earlier reports in the literature.



## 1. Introduction

### 1.1. Background

The stress analysis of wedges and sectors has been considered by a number of earlier investigators. These investigations may be grouped into two major categories: those primarily dealing with wedges and sectors with no defects, and those studying wedges and sectors with single or multiple defects. Within the first category, the problem of anti-plane stress analysis of an isotropic and dissimilar finite wedge, with different boundary conditions under point tractions on the wedge straight edges, was originally studied by Karegarnovin et al. (1997) and Kargarnovin and Fariborz (2000) A finite Mellin transform was used to analyze the wedge problem, and subsequently the geometric and loading singularities were investigated. Similarly, the stress analysis of an anisotropic finite wedge under anti-plane deformation was studied by Shahani (1999). Using the above-mentioned stress field and changing only the apex angle of finite wedge, the stress intensity factor (SIF) due to an edge crack in circular shafts and also the stress concentration factor in the apex of bonded wedges as well as bonded half planes were evaluated. More recently, the stress concentration factor for a double cantilever beam (DCB) was extracted by Shahani (2003). Solutions of dissimilar isotropic wedges subjected to anti-plane point forces and screw dislocations were studied by Lin and Ma (2004) using the Mellin transform and an image method. It was assumed that wedges with equal apex angles are attached to each other along their interface. Various boundary conditions on the wedge edges were considered and with the aid of the Peach–Koehler equation, the stress field of the image forces exerted on screw dislocations was derived. The solution of an isotropic sector wedge subjected to anti-plane shear loading on a circular edge of the wedge was obtained by Chen and Wang (2009). Different boundary conditions including fixed and traction free conditions were considered for straight edges of the finite wedge. A combination of the finite Mellin transform and the Laplace transform was used to solve the ensuing governing equations. Finally, the stress concentration of the wedge apex was studied for different edge boundary conditions.

Wedges and sectors weakened by *multiple* defects have been the subject of other earlier investigations. The anti-plane stress analysis of an infinite wedge weakened by a finite number of collinear cracks located on the wedge bisector was first studied by Mkhitaryan et al. (2001). The anti-symmetric mixed boundary conditions on both wedge faces were the specified displacement and stress components on the nonintersecting intervals. A closed-form solution of the ensuing mixed boundary problem was derived using the Mellin integral transformation in conjunction with the singular integral equations, and the crack opening and SIF on cracks tips were calculated. Anti-plane stress analysis of an infinite wedge weakened by multiple cracks with an arbitrary smooth shape and orientation was also investigated by Faal et al. (2004). The Mellin transform was used to solve the problem and the stress field of an uncracked wedge under point traction on the wedge edges was obtained. In another report by Faal et al. (2007), the Mellin transform in conjunction with an image method was used

* Corresponding author. Tel.: +98 241 515 2600; fax: +98 241 515 2762.
*E-mail address:* faal92@yahoo.com (R.T. Faal).

0020-7683/$ - see front matter © 2012 Elsevier Ltd. All rights reserved.
http://dx.doi.org/10.1016/j.ijsolstr.2012.07.013

to analyze the anti-plane stress field of a finite wedge weakened by multiple cavities. Similarly, the stress field of an undamaged finite wedge under concentrated traction on the edges was attained. In both aforementioned works, various types of boundary conditions were considered. Anti-plane stress analysis of an anisotropic finite wedge weakened by a single radial crack was the subject of the study by Shahani and Ghadiri (2010). The governing equation of the problem was rewritten in a complex form by introducing appropriate complex variables, and the solution was obtained in terms of complex functions using a set of finite complex transformations (also see Lekhnitskii, 1963; Shahani, 1999). The latter complex method may be analogous to the standard finite Mellin transforms of the first and second types. The ensuing singular dual integral equations were solved numerically to calculate the stress intensity factors at the wedge crack tips.

The anti-plane stress analysis of two different types of dissimilar sectors, i.e. the sector consisting of two isotropic sectors with the circular or the radial interface, was accomplished by Faal and Pasrad (in press a). Using the finite Fourier cosine transform as well as the technique of separation of variables, the closed-form solutions were obtained for the displacement and stress fields in each sector.

Anti-plane deformation of a typical dissimilar sector, consisting of two sub-sectors with a circular interface, was the subject of study by Faal and Pasrad (in press b). Using the finite Fourier cosine transform, the exact closed-form solutions for the displacement and stress fields of a Volterra type screw dislocation were attained. Next, using a distributed dislocation method, singular integral equations of the dissimilar sector weakened by defects (located in one of the sub-sectors) were obtained. The governing equations were found to be of the Cauchy type and solved numerically. For the sector in Faal and Pasrad (in press a), in comparison with Faal and Pasrad (in press b), an additional boundary condition was chosen such that the finite Fourier cosine transform was no longer useful and the technique of separation of variables was employed. Moreover, a new dissimilar sector, namely with the radial interface, was analyzed.

### 1.2. Motivation of this study

According to the brief review above, the stress analysis of transversely isotropic sectors weakened by multiple, arbitrarily shaped defects and with two circular fixed edges has not been the subject of previous investigations. In this article, the classical theory of elasticity for the stress analysis of a transversely isotropic sector containing Volterra-type screw dislocations is first presented (Section 2). For the simplicity of dislocation solutions, we use the dislocation arc instead of dislocation line to define the dislocation. Results in Section 2 have been validated by available dislocation solutions of isotropic finite wedges in the literature. Next, the stress analysis of a sector under point and patch loading is studied for selected boundary conditions (Section 3). Similar to Section 2, results for special cases (namely, finite wedges) have been validated by the reported data in the literature. Methodologically, Buckner's principle can be used to analyze sectors weakened by multiple cracks and cavities using the results of Sections 2 and 3. This approach is shown in Section 4. Namely, a distributed dislocation method is employed to obtain integral equations for the sector deformation and, subsequently, a set of relationships for the calculation of stress intensity factor and dimensionless hoop stress on cavities are derived in terms of the dislocation density function. Cavities are considered as closed, embedded curved cracks without singularity. Finally, a method for solving the ensuing integral equations is recommended following the work of Faal et al. (2006), where the solution of Erdogan et al. (1973) is generalized so that both cavities and embedded/edge cracks can be taken into account simultaneously. Numerical examples are presented in Section 5 and results are compared to those of an isotropic infinite wedge. Concluding remarks are included in Section 6.

In practice, the analysis of transversely isotropic sectors with multiple defects may be used, e.g., during the design of cylindrical components with unidirectional composite materials where pre-imposed defects can be present due to poor distribution of resin in a pultrosion process, etc. Other potential application areas may include piezoelectric devices made of transversely isotropic materials such as lead zirconate (PZT-4) and barium titanate ceramics, as well as transversely isotropic biological tissues such as muscle.

## 2. Problem formulation

In crack problems, a so called 'distributed dislocation technique' is often used in treating cracks with smooth geometries (Hills et al., 1996). The method relies on knowledge of the stress field due to a single dislocation in the region of interest. For a transversely isotropic sector containing a screw dislocation, the method can be developed under anti-plane deformation as follows.

Let us consider a transversely isotropic sector (Fig. 1(a)) with inner and outer radii $R_1$ and $R_2$, and sector angle $\alpha$. The origin of the polar coordinate is located at the center of the sector's circular edges and the angle $\theta$ is measured from the lower edge. As such, the sector consists of two sub-sectors $R_1 \leqslant r \leqslant a$ and $a \leqslant r \leqslant R_2$, which are attached together along the circular arc $r = a$. The only nonzero displacement component under anti-plane deformation is the out-of-plane component $w(r,\theta)$ in each region. The equilibrium equation in the absence of body forces in the polar coordinates is written as follows:

$$\frac{\partial \tau_{rz}}{\partial r} + \frac{1}{r}\frac{\partial \tau_{\theta z}}{\partial \theta} + \frac{\tau_{rz}}{r} = 0 \tag{1}$$

The constitutive equations for non-vanishing stress components are:

$$\begin{aligned} \tau_{rz} &= G_{rz}\frac{\partial w}{\partial r} \\ \tau_{\theta z} &= G_{\theta z}\frac{1}{r}\frac{\partial w}{\partial \theta} \end{aligned} \tag{2}$$

where $G_{rz}$ and $G_{\theta z}$ are the orthotropic shear moduli of the sector (Lekhnitskii, 1963). Substituting Eq. (2) into Eq. (1) leads to:

$$r^2\frac{\partial^2 w}{\partial r^2} + r\frac{\partial w}{\partial r} + G^2\frac{\partial^2 w}{\partial \theta^2} = 0 \tag{3}$$

where $G = \sqrt{\frac{G_{\theta z}}{G_{rz}}}$. The finite Fourier cosine transform for a sufficiently regular function $f(\theta)$ is defined as:

$$F(n) = \int_0^{\alpha} f(\theta)\cos\frac{n\pi\theta}{\alpha}d\theta \tag{4}$$

The inverse of the finite Fourier cosine transform yields:

$$f(\theta) = \frac{2}{\alpha}\sum_{n=1}^{\infty}F(n)\cos\frac{n\pi\theta}{\alpha} \tag{5}$$

The traction-free condition on the sector straight edges and also the fixed-edge conditions at the edges $r = R_1$ and $r = R_2$ imply that:

$$\begin{aligned} &\frac{\partial w(r,0)}{\partial \theta} = 0 \\ &\frac{\partial w(r,\alpha)}{\partial \theta} = 0 \\ &w(R_1,\theta) = 0 \\ &w(R_2,\theta) = 0 \end{aligned} \tag{6}$$

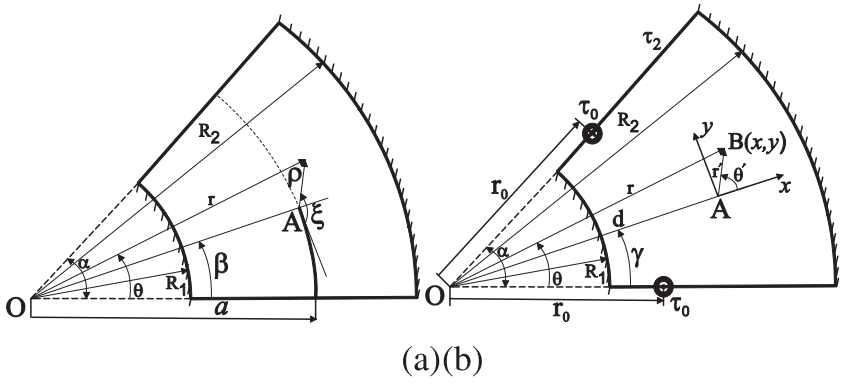


**Fig. 1.** (a) Sector with screw dislocation and (b) sector under anti-plane loading.

Application of the finite Fourier cosine transform (4) into Eq. (3) and using the boundary conditions (6) lead to:

$$r^2\frac{\partial^2 W(r,n)}{\partial r^2}+r\frac{\partial W(r,n)}{\partial r}-(n\kappa)^2 W(r,n)=0 \tag{7}$$

where $\kappa=\frac{\pi G}{\alpha}$. The general solution of Eq. (7) is:

$$W(r,n)=A_{kn}r^{n\kappa}+B_{kn}r^{-n\kappa},\quad k=1,2 \tag{8}$$

Constants $A_{kn}$ and $B_{kn}$ should be determined by applying the appropriate boundary and continuity conditions. The index $k=1,2$ is used to refer to the closer and farther sectors to the origin $O$, respectively (Fig. 1(a)). By virtue of Eqs. (5) and (8), the out of plane component $w(r,\theta)$ is written as:

$$w(r,\theta)=\frac{2}{\alpha}\sum_{n=1}^{\infty}(A_{kn}r^{n\kappa}+B_{kn}r^{-n\kappa})\cos\frac{n\pi\theta}{\alpha},\quad k=1,2 \tag{9}$$

A Volterra type screw dislocation with Burgers vector $\delta$ is situated at point $(a,\beta)$ with the dislocation arc $r=a,\ 0\leqslant\theta\leqslant\beta$. Here we use a dislocation arc instead of a dislocation line (see Faal et al., 2004, 2007, 2011) to define the dislocation. The boundary condition representing an arc dislocation under anti-plane deformation reads:

$$w(a^-,\theta)-w(a^+,\theta)=\delta H(\beta-\theta) \tag{10}$$

where $H(\cdot)$ is the Heaviside step function. The continuity condition (self-equilibrium of stress) in the sector containing the dislocation is:

$$\tau_{rz}(a^+,\theta)=\tau_{rz}(a^-,\theta) \tag{11}$$

Applying the finite Fourier cosine transform to Eqs. (10) and (11) results in:

$$\begin{aligned}&W(a^-,n)-W(a^+,n)=(\delta\alpha/n\pi)\sin(n\pi\beta/\alpha)\\&\frac{\partial W(a^+,n)}{\partial r}-\frac{\partial W(a^-,n)}{\partial r}=0\end{aligned} \tag{12}$$

The first pair of boundary conditions (6) is readily satisfied and applying the second pair of boundary conditions (6) to Eq. (9) gives:

$$\begin{aligned}&A_{1n}R_1^{n\kappa}+B_{1n}R_1^{-n\kappa}=0\\&A_{2n}R_2^{n\kappa}+B_{2n}R_2^{-n\kappa}=0\end{aligned} \tag{13}$$

Application of the conditions (12) to Eq. (9) leads to:

$$\begin{aligned}&(A_{1n}a^{n\kappa}+B_{1n}a^{-n\kappa})-(A_{2n}a^{n\kappa}+B_{2n}a^{-n\kappa})=(\delta\alpha/n\pi)\sin(n\pi\beta/\alpha)\\&(A_{1n}a^{n\kappa}-B_{1n}a^{-n\kappa})-(A_{2n}a^{n\kappa}-B_{2n}a^{-n\kappa})=0\end{aligned} \tag{14}$$

The solution of Eqs. (13) and (14) gives:

$$\begin{aligned}A_{1n}&=(\delta\alpha/2\pi)a^{-n\kappa}\Big((a/R_2)^{2n\kappa}+1\Big)\Lambda_n\\B_{1n}&=-(\delta\alpha/2\pi)(R_1^2/a)^{n\kappa}((a/R_2)^{2n\kappa}+1)\Lambda_n\\A_{2n}&=(\delta\alpha/2\pi)a^{-n\kappa}((a/R_2)^{2n\kappa}+(R_1/R_2)^{2n\kappa})\Lambda_n\\B_{2n}&=-(\delta\alpha/2\pi)(a^{n\kappa}+(R_1^2/a)^{n\kappa})\Lambda_n\end{aligned} \tag{15}$$

where $\Lambda_n=\sin(n\pi\beta/\alpha)/n(1-(R_1/R_2)^{n\kappa})$. Substituting coefficients (15) into Eq. (9) results in:

$$\begin{aligned}&w(r,\theta)=\frac{\delta}{\pi}\sum_{n=1}^{\infty}\Lambda_n[(r/a)^{n\kappa}+(ra/R_2^2)^{n\kappa}-(aR_1^2/rR_2^2)^{n\kappa}-(R_1^2/ra)^{n\kappa}]\cos\frac{n\pi\theta}{\alpha},\\&R_1\leqslant r\leqslant a\\&w(r,\theta)=\frac{\delta}{\pi}\sum_{n=1}^{\infty}\Lambda_n[(ra/R_2^2)^{n\kappa}+(rR_1^2/aR_2^2)^{n\kappa}-(a/r)^{n\kappa}-(R_1^2/ra)^{n\kappa}]\cos\frac{n\pi\theta}{\alpha},\\&a\leqslant r\leqslant R_2\end{aligned} \tag{16}$$

Using the first equation of (16) in Eq. (2), the stress field when $R_1\leqslant r\leqslant a$ is obtained as:

$$\begin{aligned}\tau_{rz}&=GG_{rz}\frac{\delta}{\alpha r}\sum_{n=1}^{\infty}n\Lambda_n[(r/a)^{n\kappa}+(ra/R_2^2)^{n\kappa}+(aR_1^2/rR_2^2)^{n\kappa}+(R_1^2/ra)^{n\kappa}]\cos\frac{n\pi\theta}{\alpha}\\\tau_{\theta z}&=-G_{\theta z}\frac{\delta}{\alpha r}\sum_{n=1}^{\infty}n\Lambda_n[(r/a)^{n\kappa}+(ra/R_2^2)^{n\kappa}-(aR_1^2/rR_2^2)^{n\kappa}-(R_1^2/ra)^{n\kappa}]\sin\frac{n\pi\theta}{\alpha}\end{aligned} \tag{17}$$

For $a\leqslant r\leqslant R_2$, the stress component $\tau_{rz}(r,\theta)$ is achieved by replacing $r/a$ with $a/r$. Analogously, for stress component $\tau_{\theta z}(r,\theta)$, similar changes are made for each region. Moreover the changed terms are multiplied by a negative sign. Making use of the formulas given in Appendix (A) of the report by Faal et al. (2004) and the Taylor's expansion of expression $n\Lambda_n$ (i.e., $n\Lambda_n=\sin\frac{n\pi\beta}{\alpha}\sum_{m=0}^{\infty}(R_1/R_2)^{2mn\kappa}$), the stress components (17) are summed in the whole sector region, leading to:

$$\begin{aligned}\tau_{rz}=&\frac{\delta\kappa G_{rz}}{4\pi r}\sum_{m=0}^{\infty}\{[\varphi_m(r/a,\pi(\beta-\theta)/\alpha)+\varphi_m(r/a,\pi(\beta+\theta)/\alpha)]\\&+[\varphi_m(ra/R_2^2,\pi(\beta-\theta)/\alpha)+\varphi_m(ra/R_2^2,\pi(\beta+\theta)/\alpha)]\\&+[\varphi_m(aR_1^2/rR_2^2,\pi(\beta-\theta)/\alpha)+\varphi_m(aR_1^2/rR_2^2,\pi(\beta+\theta)/\alpha)]\\&+[\varphi_m(R_1^2/ra,\pi(\beta-\theta)/\alpha)+\varphi_m(R_1^2/ra,\pi(\beta+\theta)/\alpha)]\},\quad R_1\leqslant r\leqslant a\\\tau_{\theta z}=&-\frac{\delta\kappa GG_{rz}}{4\pi r}\sum_{m=0}^{\infty}\{\psi_m(r/a,\pi(\beta+\theta)/\alpha)-\psi_m(r/a,\pi(\beta-\theta)/\alpha)\\&+\psi_m(ra/R_2^2,\pi(\beta+\theta)/\alpha)-\psi_m(ra/R_2^2,\pi(\beta-\theta)/\alpha)\\&-\psi_m(aR_1^2/rR_2^2,\pi(\beta+\theta)/\alpha)+\psi_m(aR_1^2/rR_2^2,\pi(\beta-\theta)/\alpha)\\&-\psi_m(R_1^2/ra,\pi(\beta+\theta)/\alpha)+\psi_m(R_1^2/ra,\pi(\beta-\theta)/\alpha)\},\quad R_1\leqslant r\leqslant a\end{aligned} \tag{18}$$

where $\eta=R_1/R_2$ and

$$\varphi_m(x,\theta,\kappa,\eta)=\frac{\sin\theta}{\cosh\{\kappa[2mLn\eta+Lnx]\}-\cos\theta}$$
$$\psi_m(x,\theta,\kappa,\eta)=\frac{\sinh\{\kappa[mLn\eta+Lnx]\}}{\cosh\{\kappa[2mLn\eta+Lnx]\}-\cos\theta} \tag{19}$$

For brevity, the constants $\kappa$ and $\eta$ were eliminated from Eq. (18). For finite wedges, $R_1=0$ then $\eta=0$ and the functions $\varphi_m(x,\theta,\kappa,\eta)$ and $\psi_m(x,\theta,\kappa,\eta)$ are vanished for all $m\neq 0$. Therefore, the stress field (18) is simplified for a finite wedge as follows:

$$\begin{aligned}\tau_{rz}&=\frac{\delta\kappa G_{rz}}{4\pi r}[\phi_0(r/a,\pi(\beta-\theta)/\alpha)+\phi_0(r/a,\pi(\beta+\theta)/\alpha)\\&\quad+\phi_0(ra/R_2^2,\pi(\beta-\theta)/\alpha)+\phi_0(ra/R_2^2,\pi(\beta+\theta)/\alpha)],\quad 0\leqslant r\leqslant a\\\tau_{\theta z}&=\frac{\delta\kappa G G_{rz}}{4\pi r}[-\psi_0(r/a,\pi(\beta+\theta)/\alpha)+\psi_0(r/a,\pi(\beta-\theta)/\alpha)\\&\quad-\psi_0(ra/R_2^2,\pi(\beta+\theta)/\alpha)+\psi_0(ra/R_2^2,\pi(\beta-\theta)/\alpha)],\quad 0\leqslant r\leqslant a\end{aligned} \tag{20}$$

Comparing the above stress field to the solution obtained by Faal et al. (2007) and performing some manipulations show identical results. It is also worth mentioning that the dislocation definition used by Faal et al. (2007) was based on a straight cut of the wedge, but here we employ a circular cut to define the dislocation. One of the benefits of using a circular cut is the simplicity of finding the dislocation solution. To investigate the behavior of stress fields in the dislocation position, let us define a new coordinate system $(\rho,\xi)$, Fig. 1(a). The relationships between the two coordinates may be written as:

$$r=\sqrt{a^2+\rho^2+2a\rho\sin\xi},$$
$$\theta=\beta-\sin^{-1}\left(\frac{\rho\cos\xi}{\sqrt{a^2+\rho^2+2a\rho\sin\xi}}\right),\qquad 0\leqslant\xi\leqslant 2\pi \tag{21}$$

Substituting (21) into $\varphi_0(r/a,\pi(\beta-\theta)/\alpha)$ and $\psi_0(r/a,\pi(\beta-\theta)/\alpha)$ and carrying out the necessary manipulations yields:

$$\begin{aligned}\frac{1}{r}\varphi_0(r/a,\pi(\beta-\theta)/\alpha)&\sim\frac{2\alpha}{\pi\cos\xi}\frac{1}{\rho},\quad\text{as }\rho\to 0,\ 0\leqslant\xi\leqslant 2\pi\\\frac{1}{r}\psi_0(r/a,\pi(\beta-\theta)/\alpha)&\sim\frac{G\alpha\sin\xi}{2\pi\cos^2\xi}\frac{1}{\rho},\quad\text{as }\rho\to 0,\ 0\leqslant\xi\leqslant 2\pi\end{aligned} \tag{22}$$

According to the above relations, one can conclude that $(\tau_{rz},\tau_{\theta z})\sim\frac{1}{\rho}$ as $\rho\to 0$. It should be added that this Cauchy singularity was previously reported, e.g., by Weertman and Weertman (1992) for the stress field of two-dimensional isotropic media containing screw dislocations. It has also been reported by Faal et al. (2006, 2011) for the stress field of an orthotropic strip and rectangular planes containing screw dislocations.

## 3. Transversely isotropic sector under traction

In this section we use the analysis framework of Section 2 and predict the anti-plane deformation of a transversely isotropic sector under two point forces/tractions with a magnitude of $\tau_0$ (Fig. 1(b)). The boundary conditions (6) hold but the first two boundary conditions should be replaced by:

$$\tau_{\theta z}(r,0)=\tau_{\theta z}(r,\alpha)=\tau_0\delta(r-r_0) \tag{23}$$

where $\delta(\cdot)$ is Dirac delta function. Application of the finite Fourier cosine transform (4) to Eq. (3) and recalling the boundary conditions (23)leads to:

$$\begin{aligned}&r^2\frac{\partial^2 W(r,n)}{\partial r^2}+r\frac{\partial W(r,n)}{\partial r}-(n\kappa)^2W(r,n)\\&\quad=(r\tau_0/G_{\theta z})[1+(-1)^{n+1}]\delta(r-r_0)\end{aligned} \tag{24}$$

Solving Eq. (24) as a Green's function problem leads to seeking a $W(r,n)$ as follows:

$$\begin{cases}W(r,n)=C_1r^{n\kappa}+D_1r^{-n\kappa} & R_1\leqslant r\leqslant r_0\\ W(r,n)=C_2r^{n\kappa}+D_2r^{-n\kappa} & r_0\leqslant r\leqslant R_2\end{cases} \tag{25}$$

Continuity of displacements at $r=r_0$ imply that:

$$W(r_0^-,n)=W(r_0^+,n) \tag{26}$$

Application of the last two boundary conditions (6) and continuity equations of (26) to (25) in view of (5) gives:

$$\begin{aligned}&C_1R_1^{n\kappa}+D_1R_1^{-n\kappa}=0\\&C_2R_2^{n\kappa}+D_2R_2^{-n\kappa}=0\\&C_1r_0^{n\kappa}+D_1r_0^{-n\kappa}=C_2r_0^{n\kappa}+D_2r_0^{-n\kappa}\end{aligned} \tag{27}$$

Integrating Eq. (24) over the arc $r=r_0$ gives:

$$\begin{aligned}&\int_{r_0^-}^{r_0^+}r^2\frac{\partial^2W(r,n)}{\partial r^2}dr+\int_{r_0^-}^{r_0^+}r\frac{\partial W(r,n)}{\partial r}dr-(n\kappa)^2\int_{r_0^-}^{r_0^+}W(r,n)\,dr\\&\qquad=\frac{\tau_0}{G_{\theta z}}[1+(-1)^{n+1}]\int_{r_0^-}^{r_0^+}r\delta(r-r_0)\,dr\end{aligned} \tag{28}$$

Considering the fact that the displacement is continuous along the arc $r=r_0$ and making use of the integration by parts, Eq. (28) is simplified to:

$$\frac{\partial W(r_0^+,n)}{\partial r}-\frac{\partial W(r_0^-,n)}{\partial r}=(\tau_0/r_0G_{\theta z})[1+(-1)^{n+1}] \tag{29}$$

Application of conditions (29) to Eq. (25) leads to:

$$(C_2r_0^{n\kappa}-D_2r_0^{-n\kappa})-(C_1r_0^{n\kappa}-D_1r_0^{-n\kappa})=(\tau_0/n\kappa r_0G_{\theta z})\left[1+(-1)^{n+1}\right] \tag{30}$$

The solution of Eqs. (27) and (30) results in the coefficients $C_1$, $D_1$, $C_2$ and $D_2$ and, by substituting those into Eq. (25) and applying the inverse transform (5) to the ensuing equations, leads to the displacement field as:

$$\begin{aligned}w(r,\theta)&=\frac{\tau_0}{\pi GG_{\theta z}}\sum_{n=1}^{\infty}(1+(-1)^{n+1})\Gamma_n\left[\left(rr_0/R_2^2\right)^{n\kappa}-(r/r_0)^{n\kappa}+\left(R_1^2/rr_0\right)^{n\kappa}\right.\\&\quad\left.-\left(R_1^2r_0/R_2^2r\right)^{n\kappa}\right]\cos\frac{n\pi\theta}{\alpha},\quad R_1\leqslant r\leqslant r_0\\w(r,\theta)&=\frac{\tau_0}{\pi GG_{\theta z}}\sum_{n=1}^{\infty}(1+(-1)^{n+1})\Gamma_n\left[\left(r_0r/R_2^2\right)^{n\kappa}-(R_1^2r/R_2^2r_0)^{n\kappa}\right.\\&\quad\left.+\left(R_1^2/r_0r\right)^{n\kappa}-(r_0/r)^{n\kappa}\right]\cos\frac{n\pi\theta}{\alpha},\quad r_0\leqslant r\leqslant R_2\end{aligned} \tag{31}$$

where $\Gamma_n=1/n(1-(R_1/R_2)^{2n\kappa})=\Lambda_n/\sin(n\pi\beta/\alpha)$. Stress components in the whole sector region are attained in view of the constitutive Eq. (2) as follows:

$$\begin{aligned}\tau_{rz}(r,\theta)&=\frac{\tau_0}{G^2\alpha r}\sum_{n=1}^{\infty}n(1+(-1)^{n+1})\Gamma_n[\left(r_0r/R_2^2\right)^{n\kappa}-(r/r_0)^{n\kappa}\\&\quad-\left(R_1^2/r_0r\right)^{n\kappa}+(R_1^2r/R_2^2r_0)^{n\kappa}]\cos\frac{n\pi\theta}{\alpha},\quad R_1\leqslant r\leqslant r_0\\\tau_{\theta z}(r,\theta)&=-\frac{\tau_0}{G\alpha r}\sum_{n=1}^{\infty}n(1+(-1)^{n+1})\Gamma_n[\left(r_0r/R_2^2\right)^{n\kappa}-(r/r_0)^{n\kappa}\\&\quad+\left(R_1^2/r_0r\right)^{n\kappa}-(R_1^2r_0/R_2^2r)^{n\kappa}]\sin\frac{n\pi\theta}{\alpha},\quad R_1\leqslant r\leqslant r_0\end{aligned} \tag{32}$$

For $r_0\leqslant r\leqslant R_2$, the stress component $\tau_{\theta z}(r,\theta)$ is achieved by replacing $r/r_0$ with $r_0/r$. Analogously for the stress component $\tau_{rz}(r,\theta)$, similar changes are done for each region. Moreover, the changed terms were multiplied by a negative sign. The term $n\Gamma_n$ is replaced by the series $\sum_{m=0}^{\infty}(R_1/R_2)^{2mn\kappa}$ and the stress components are

summed using the relationships given in Appendix (A) of Faal et al. (2004).

$$\begin{aligned}\tau_{rz}(r,\theta)=&\frac{\tau_0}{2G^2\alpha r}\sum_{m=0}^{\infty}[\psi_m\left(r_0r/R_2^2,\pi-\pi\theta/\alpha\right)-\psi_m\left(r_0r/R_2^2,\pi\theta/\alpha\right)\\&-\psi_m(r/r_0,\pi-\pi\theta/\alpha)+\psi_m(r/r_0,\pi\theta/\alpha)-\psi_m\left(R_1^2/r_0r,\pi-\pi\theta/\alpha\right)\\&+\psi_m\left(R_1^2/r_0r,\pi\theta/\alpha\right)+\psi_m\left(R_1^2r/R_2^2r_0,\pi-\pi\theta/\alpha\right)\\&-\psi_m\left(R_1^2r/R_2^2r_0,\pi\theta/\alpha\right)],\quad R_1\leqslant r\leqslant r_0\\\tau_{\theta z}(r,\theta)=&-\frac{\tau_0}{2G\alpha r}\sum_{m=0}^{\infty}\Big\{\varphi_m\left(r_0r/R_2^2,\pi\theta/\alpha\right)+\varphi_m\left(r_0r/R_2^2,\pi-\pi\theta/\alpha\right)\\&-\varphi_m(r/r_0,\pi\theta/\alpha)-\varphi_m(r/r_0,\pi-\pi\theta/\alpha)+\varphi_m\left(R_1^2/r_0r,\pi\theta/\alpha\right)\\&+\varphi_m\left(R_1^2/r_0r,\pi-\pi\theta/\alpha\right)-\varphi_m\left(R_1^2r_0/R_2^2r,\pi\theta/\alpha\right)\\&-\varphi_m\left(R_1^2r_0/R_2^2r,\pi-\pi\theta/\alpha\right)\Big\},\quad R_1\leqslant r\leqslant r_0\end{aligned}\tag{33}$$

It can be seen that the displacement and stress fields satisfy the prescribed boundary and continuity conditions. For $R_1=0$ and $G_{\theta z}=G_{rz}$, Eq. (33) are simplified and the stress field of reference (Faal et al., 2007) is achieved. The local coordinates $(r',\theta')$, Fig. 1(b), is moved to the load location as $\theta=\sin^{-1}(r'\sin\theta'/r)$, $0\leqslant\theta'\leqslant\pi$ and $r=\sqrt{r'^2+r_0^2+2r'r_0\cos\theta'}$. Using this transformation we deduce that $(\tau_{rz},\tau_{\theta z})\sim 1/r'$ near the traction $\tau_0$ i.e. $r'\to 0$. Choosing similar local coordinates in the sector corners, it can be shown that the stress is not singular. These corners can be modeled by a rectangular wedge apex which is not singular, confirming the report by Karegarnovin et al. (1997) for isotropic wedges.

## 4. Transversely isotropic sector with multiple cracks and cavities

The dislocation solution accomplished in Section 3 may be extended to analyze sectors with multiple defects consisting of cracks and cavities. The cavities are considered as closed-curve cracks without singularity. Consequently, the analysis resembles that of Faal et al. (2004, 2007, 2011) but with overriding the crack singularity. We consider a sector weakened by $M$ cavities, $N_1$ embedded cracks, and $N_2$ edge cracks. Henceforth, we designate cavities, embedded cracks and edge cracks with the respective subscripts as follows.

$$\begin{aligned}&i\in\{1,2,\ldots,M\}\\&j\in\{M+1,M+2,\ldots,M+N_1\}\\&k\in\{M+N_1+1,M+N_1+2,\ldots,M+N_1+N_2\}\end{aligned}$$

where $N=M+N_1+N_2$ and represents the total number of defects. The antiplane traction on the surface of the $i$-th defect, $i=1,2,\ldots,N$, Fig. 2, in terms of stress components in polar coordinates becomes:

$$\begin{aligned}\tau_{tz}(r_i,\theta_i)&=\tau_{\theta z}(r_i,\theta_i)\sin\phi_i+\tau_{rz}(r_i,\theta_i)\cos\phi_i\\\tau_{nz}(r_i,\theta_i)&=\tau_{\theta z}(r_i,\theta_i)\cos\phi_i-\tau_{rz}(r_i,\theta_i)\sin\phi_i\end{aligned}\tag{34}$$

where $\phi_i$ is the angle between tangent to the surface of the $i$-th defect and the radial direction $r_i$. Suppose dislocations with unknown density $B_{zj}(r_j)$ are distributed on the infinitesimal segment at the boundary of the $j$-th defect. The traction on the surface of the $i$-th defect due to the presence of dislocations, utilizing (34) and (18), leads to:

$$\begin{aligned}\tau_{nz}(r_i,\theta_i)=&-\frac{B_{zj}(r_j)\kappa G_{rz}}{4\pi r_i}\sum_{m=0}^{\infty}\{\sin\phi_i\{\varphi_m(r_i/r_j,\pi(\theta_j-\theta_i)/\alpha)\\&+\varphi_m(r_i/r_j,\pi(\theta_j+\theta_i)/\alpha)+\varphi_m\left(r_ir_j/R_2^2,\pi(\theta_j-\theta_i)/\alpha\right)\\&+\varphi_m\left(r_ir_j/R_2^2,\pi(\theta_j+\theta_i)/\alpha\right)+\varphi_m\left(r_jR_1^2/r_iR_2^2,\pi(\theta_j-\theta_i)/\alpha\right)\\&+\varphi_m\left(r_jR_1^2/r_iR_2^2,\pi(\theta_j+\theta_i)/\alpha\right)+\varphi_m\left(R_1^2/r_ir_j,\pi(\theta_j-\theta_i)/\alpha\right)\\&+\varphi_m\left(R_1^2/r_ir_j,\pi(\theta_j+\theta_i)/\alpha\right)\}+G\{\psi_m(r_i/r_j,\pi(\theta_j+\theta_i)/\alpha)\\&-\psi_m(r_i/r_j,\pi(\theta_j-\theta_i)/\alpha)+\psi_m\left(r_ir_j/R_2^2,\pi(\theta_j+\theta_i)/\alpha\right)\\&-\psi_m\left(r_ir_j/R_2^2,\pi(\theta_j-\theta_i)/\alpha\right)-\psi_m\left(r_jR_1^2/r_iR_2^2,\pi(\theta_j+\theta_i)/\alpha\right)\\&+\psi_m\left(r_jR_1^2/r_iR_2^2,\pi(\theta_j-\theta_i)/\alpha\right)-\psi_m\left(R_1^2/r_ir_j,\pi(\theta_j+\theta_i)/\alpha\right)\\&+\psi_m\left(R_1^2/r_ir_j,\pi(\theta_j-\theta_i)/\alpha\right)\}\cos\phi_i\}\sqrt{(dr_j)^2+(r_jd\theta_j)^2};\\&R_1\leqslant r_i\leqslant r_j\end{aligned}\tag{35}$$

For $r_j\leqslant r_i\leqslant R_2$, the traction $\tau_{nz}(r_i,\theta_i)$ is written through the replacement of the term $r_i/r_j$ by $r_j/r_i$ and multiplying the functions $\psi_m$ by a negative sign. Covering the boundary of cavities or border of cracks by dislocations, the principle of superposition may used to obtain traction on the surface of cavities or cracks. Equation set (35) is integrated on the boundary of defects and the resultant tractions are superimposed. The integration of Eq. (35) can be facilitated by describing the configuration of cracks and cavities in a parametric form. For example, the parameter $-1\leqslant s\leqslant 1$ is chosen and the following change of variables is employed for elliptical cavities with major and minor semi-axes $a_i$ and $b_i$, respectively,

$$\begin{aligned}r_i(s)&=\left\{d_i^2+a_i^2b_i^2/\left[b_i^2\cos^2(\pi s+\omega_{si})+a_i^2\sin^2(\pi s+\omega_{si})\right]-2a_ib_id_i\cos(\pi s+\omega_{si}+\psi_{si})\Big/\sqrt{b_i^2\cos^2(\pi s+\omega_{si})+a_i^2\sin^2(\pi s+\omega_{si})}\right\}^{\frac{1}{2}}\\\theta_i(s)&=\tan^{-1}\left\{d_i\sin\beta_i\sqrt{b_i^2\cos^2(\pi s+\omega_{si})+a_i^2\sin^2(\pi s+\omega_{si})}-a_ib_i\sin(\pi s+\omega_{si}+\psi_{si}+\beta_i)\Big/\left[d_i\cos\beta_i\sqrt{b_i^2\cos^2(\pi s+\omega_{si})+a_i^2\sin^2(\pi s+\omega_{si})}-a_ib_i\cos(\pi s+\omega_{si}+\psi_{si}+\beta_i)\right]\right\}\\\phi_i(s)&=\tan^{-1}[r_i(s)\theta_i'(s)/r_i'(s)]\end{aligned}\tag{36}$$

where $(d_i,\beta_i)$ is the coordinate of the cavity center and $\phi_i(s)$ is the angle between a tangent to the surface of the cavity and the radial direction $r_i(s)$. Also, $\omega_{si}$ is the angle specifying the starting point and $\psi_{si}$ is the orientation angle of the major axis (Faal et al., 2007). In Eq. (36), the prime sign indicates differentiation with respect to the function argument. The traction on the surface of the $i$-th crack or cavity in the sector containing $N$ defects may be expressed as:

$$\begin{aligned}&\tau_{nz}(r_i(s),\theta_i(s))=\sum_{j=1}^{N}\int_{-1}^{1}b_{zj}(t)k_{ij}(s,t)\,dt,\quad -1\leqslant s\leqslant 1,\\&\quad i=1,2,\ldots,N\end{aligned}\tag{37}$$

where $b_{zj}(t)$ is the dislocation density on the non-dimensional length of the boundary of the $j$-th crack or cavity. The above kernel

$k_{ij}(s,t)$ in light of Eq. (35) can be obtained as shown in Appendix A. The functions $\varphi_0(r_i(s)/r_j(t), \pi(\theta_j-\theta_i)/\alpha)$ and $\psi_0(r_i(s)/r_j(t), \pi(\theta_j-\theta_i)/\alpha)$ are singular for $i=j$ as $t\to s$. Hence, we may conclude that $k_{ij}(s,t)$ has the Cauchy-type singularity for $i=j$ as $t\to s$. By virtue of Bueckner's principle[1] (Korsunsky and Hills, 1996) the left-hand side of Eq. (37), after changing the sign, is the traction caused by the external loading on the sector without defect at the presumed boundary of cavities or crack borders. The applied traction on the sector with multiple defects is taken to be as Eq. (23) and the stress components as Eq. (33). Utilizing Eqs. (33) and (34), the following traction should be applied on the surface of the $i$-th defect:

$$\begin{aligned}\tau_{nz}(r_i(s),\theta_i(s)) = \frac{\tau_0}{2G^2\alpha r_i}\sum_{m=0}^{\infty}\Big\{G\Big[&\varphi_m\Big(r_0r_i/R_2^2, \pi\theta_i/\alpha\Big)\\ &+\varphi_m\Big(r_0r_i/R_2^2, \pi-\pi\theta_i/\alpha\Big)-\varphi_m(r_i/r_0, \pi\theta_i/\alpha)\\ &-\varphi_m(r_i/r_0, \pi-\pi\theta_i/\alpha)+\varphi_m\Big(R_1^2/r_0r_i, \pi\theta_i/\alpha\Big)\\ &+\varphi_m\Big(R_1^2/r_0r_i, \pi-\pi\theta_i/\alpha\Big)-\varphi_m\Big(R_1^2r_0/R_2^2r_i, \pi\theta_i/\alpha\Big)\\ &-\varphi_m\Big(R_1^2r_0/R_2^2r_i, \pi-\pi\theta_i/\alpha\Big)\Big]\cos\phi_i\\ &+\Big[-\psi_m\Big(r_0r_i/R_2^2, \pi-\pi\theta_i/\alpha\Big)-\psi_m\Big(r_0r_i/R_2^2, \pi\theta_i/\alpha\Big)\\ &+\psi_m(r_i/r_0, \pi-\pi\theta_i/\alpha)+\psi_m(r_i/r_0, \pi\theta_i/\alpha)\\ &+\psi_m\Big(R_1^2/r_0r_i, \pi-\pi\theta_i/\alpha\Big)+\psi_m\Big(R_1^2/r_0r_i, \pi\theta_i/\alpha\Big)\\ &-\psi_m\Big(R_1^2r_i/R_2^2r_0, \pi-\pi\theta_i/\alpha\Big)\\ &-\psi_m\Big(R_1^2r_i/R_2^2r_0, \pi\theta_i/\alpha\Big)\Big]\sin\phi_i\Big\};\quad R_1\leqslant r_i\leqslant r_0\end{aligned}$$

$$\begin{aligned}\tau_{nz}(r_i(s),\theta_i(s)) = \frac{\tau_0}{2G^2\alpha r_i}\sum_{m=0}^{\infty}\Big\{G\Big[&\varphi_m\Big(r_0r_i/R_2^2, \pi\theta_i/\alpha\Big)\\ &+\varphi_m\Big(r_0r_i/R_2^2, \pi-\pi\theta_i/\alpha\Big)-\varphi_m\Big(R_1^2r_i/R_2^2r_0, \pi-\pi\theta_i/\alpha\Big)\\ &-\varphi_m\Big(R_1^2r_i/R_2^2r_0, \pi\theta_i/\alpha\Big)+\varphi_m\Big(R_1^2/r_0r_i, \pi\theta_i/\alpha\Big)\\ &+\varphi_m\Big(R_1^2/r_0r_i, \pi-\pi\theta_i/\alpha\Big)-\varphi_m(r_0/r_i, \pi\theta_i/\alpha)\\ &-\varphi_m(r_0/r_i, \pi-\pi\theta_i/\alpha)]\cos\phi_i\\ &+\Big[-\psi_m\Big(r_0r_i/R_2^2, \pi-\pi\theta_i/\alpha\Big)-\psi_m\Big(r_0r_i/R_2^2, \pi\theta_i/\alpha\Big)\\ &+\psi_m\Big(R_1^2r_i/R_2^2r_0, \pi-\pi\theta_i/\alpha\Big)+\psi_m\Big(R_1^2r_i/R_2^2r_0, \pi\theta_i/\alpha\Big)\\ &+\psi_m\Big(R_1^2/r_0r_i, \pi-\pi\theta_i/\alpha\Big)+\psi_m\Big(R_1^2/r_0r_i, \pi\theta_i/\alpha\Big)\\ &-\psi_m(r_0/r_i, \pi-\pi\theta_i/\alpha)\\ &-\psi_m(r_0/r_i, \pi\theta_i/\alpha)]\sin\phi_i\Big\};\quad r_0\leqslant r_i\leqslant R_2\end{aligned}\tag{38}$$

Employing the definition of a dislocation density function, the equation for crack opening displacement across the $j$-th crack is:

$$w_j^+(s)-w_j^-(s)=\int_{-1}^{s}\sqrt{\Big(r_j'(t)\Big)^2+\Big(r_j(t)\theta_j'(t)\Big)^2}\,b_{zj}(t)\,dt,\quad -1\leqslant s\leqslant 1,\ \ j=1,2,\ldots,N\tag{39}$$

The uniqueness requirement of a displacement field on the surfaces of cavities and embedded crack borders implies:

$$\int_{-1}^{1}\sqrt{\Big(r_j'(t)\Big)^2+\Big(r_j(t)\theta_j'(t)\Big)^2}\,b_{zj}(t)\,dt=0,\quad j=1,2,\ldots,M+N_1\tag{40}$$

The Cauchy singular integral Eqs. (37) and (40) are solved simultaneously to determine dislocation density functions. Cavities are defined as closed curved cracks with a bounded dislocation density at both ends of the cracks. Thus, for $-1\leqslant t\leqslant 1$, $j=1,2,\ldots,M$ the dislocation density functions for cavities are expressed as:

$$b_{zj}(t)=g_{zj}(t)\sqrt{1-t^2}\tag{41}$$

Stress fields for embedded cracks in orthotropic media are singular at crack tips with square root singularity (Delale, 1984). To show the order of stress singularity for embedded cracks located at the transversely isotropic sector, we selected a local coordinate $(x,y)$ or $(r',\theta')$ as $x,y\to 0$ or $r'\to 0$, see Fig. 1(b). Following, the transformation between the two coordinate systems $(x,y)$ or $(r,\theta)$ is written as:

$$\begin{aligned}x&=r\cos(\theta-\gamma)-d\\ y&=r\sin(\theta-\gamma)\end{aligned}\tag{42}$$

Application of the above transformation to Eq. (3) yields:

$$\begin{aligned}&(x+d)^2\frac{\partial^2 w}{\partial x^2}+y^2\frac{\partial^2 w}{\partial y^2}+2y(x+d)\frac{\partial^2 w}{\partial x\partial y}+(x+d)\frac{\partial w}{\partial x}+y\frac{\partial w}{\partial y}\\ &+G^2\left[y^2\frac{\partial^2 w}{\partial x^2}+(x+d)^2\frac{\partial^2 w}{\partial y^2}-2y(x+d)\frac{\partial^2 w}{\partial x\partial y}-y\frac{\partial w}{\partial y}-(x+d)\frac{\partial w}{\partial x}\right]=0\end{aligned}\tag{43}$$

For $x,y\to 0$ the above equation is approximated by:

$$\frac{\partial^2 w}{\partial x^2}+G^2\frac{\partial^2 w}{\partial y^2}=0\tag{44}$$

Now let us make a comparison. We consider an orthotropic material where the shear modulus in the $x$-direction ($G_{xz}$) is different from that in the $y$-direction ($G_{yz}$). The governing equation of this material under anti-plane deformation is $G_{xz}\frac{\partial^2 w}{\partial x^2}+G_{yz}\frac{\partial^2 w}{\partial y^2}=0$ (Liebowitz, 1968). The interesting observation is that we are able to compare this equation with Eq. (44) by defining $G=\sqrt{G_{yz}/G_{xz}}$. The displacement field of a transversely isotropic sector, which is globally governed by Eq. (3) through the coordinates $(r,\theta)$ is locally governed by Eq. (44). We recall that Eq. (44) is valid only for the infinitesimal neighborhood of point $A(r,\theta)$. Therefore in the vicinity of each specified point of the transversely isotropic sector we may assume an orthotropic material with the governing equation $G_{xz}\frac{\partial^2 w}{\partial x^2}+G_{yz}\frac{\partial^2 w}{\partial y^2}=0$, but the material properties $G_{xz}$ and $G_{yz}$ should be replaced by $G_{rz}$ and $G_{\theta z}$, respectively. Let us consider a crack tip located at the point $(x,y)$ of an orthotropic sector ($G_{xz}\neq G_{yz}$). The displacement and stress distributions around the crack tip are given in the study by Liebowitz (1968) by solving the equation $G_{xz}\frac{\partial^2 w}{\partial x^2}+G_{yz}\frac{\partial^2 w}{\partial y^2}=0$. For brevity, we give only the displacement field solution as:

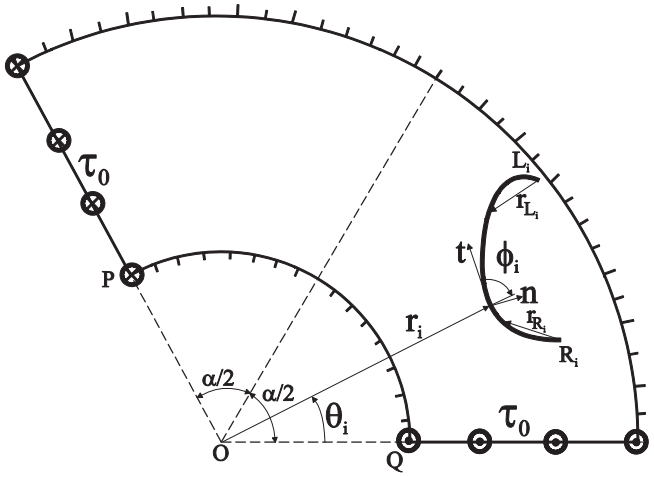


**Fig. 2.** Schematic view of the sector with a smooth curved crack.

[1] If a cracked body includes forces applied to the crack surfaces to close it (or slide for the modes II and III of fracture mechanics), while the body is subjected to an external loading or prescribed displacement at its boundary, the applied forces to the crack surfaces must be equivalent to the stress distribution in an uncracked body of the same geometry subject to the same external loading.

$$w(x,y) = k_{III}\sqrt{2/G_{xz}G_{yz}}\,Im\left[\sqrt{x+(y/G)i}\right] \tag{45}$$

where $G = \sqrt{G_{yz}/G_{xz}}$ and $k_{III}$ is the stress intensity factor of the tearing mode of fracture. The equation above is also valid for the infinitesimal neighborhood of each specified point of the transversely isotropic sector, but the material properties $G_{xz}$ and $G_{yz}$ are replaced by $G_{rz}$ and $G_{\theta z}$, respectively. In view of Fig. 1(b), we have $x = r'\cos\theta'$ and $y = r'\sin\theta'$. Consequently, it is straightforward to deduce that the stress field in the crack tip has a square root singularity. Thus, the dislocation density functions are represented by $-1 \leqslant t \leqslant 1$, $j = M+1, 2, \ldots, M+N_1$ as

$$b_{zj}(t) = g_{zj}(t)/\sqrt{1-t^2} \tag{46}$$

Following, Eq. (45) is rewritten for a crack tip located at the point $A(r,\theta)$ of the transversely isotropic sector, Fig. 1(b), as follows:

$$w(x,y) = k_{III}\sqrt{2/G_{rz}G_{\theta z}}\,Im\left[\sqrt{x+(y/G)i}\right] \tag{47}$$

Thus, the stress intensity factors for the $i$-th crack in terms of crack opening displacement are:

$$\begin{aligned} k_{IIILi} &= \frac{\sqrt{2}}{4}GG_{rz}\lim_{r_{L_i}\to 0}\frac{w^+(s)-w^-(s)}{\sqrt{r_{L_i}}},\\ k_{IIIRi} &= \frac{\sqrt{2}}{4}GG_{rz}\lim_{r_{R_i}\to 0}\frac{w^+(s)-w^-(s)}{\sqrt{r_{R_i}}} \end{aligned} \tag{48}$$

for $i = M+1, 2, \ldots, N$, where $r$ is the distance from a crack tip. Setting the points $L_i$ and $R_i$ on the surface of the crack, as shown in Fig. 2, yields:

$$\begin{aligned} r_{L_i} &= \sqrt{(r_i(s))^2 + (r_i(-1))^2 - 2r_i(s)r_i(-1)\cos(\theta_i(s)-\theta_i(-1))}\\ r_{R_i} &= \sqrt{(r_i(s))^2 + (r_i(1))^2 - 2r_i(s)r_i(1)\cos(\theta_i(s)-\theta_i(1))} \end{aligned} \tag{49}$$

Substituting Eq. (46) into Eq. (39), and Eq. (49) into Eq. (48), and finally employing L'Hopital's rule yields the stress intensity factors for the embedded cracks:

$$\begin{aligned} k_{IIILi} &= \frac{1}{2}GG_{rz}[(r_i'(-1))^2 + (r_i(-1)\theta_i'(-1))^2]^{\frac{1}{4}}g_{zi}(-1)\\ k_{IIIRi} &= -\frac{1}{2}GG_{rz}[(r_i'(1))^2 + (r_i(1)\theta_i'(1))^2]^{\frac{1}{4}}g_{zi}(1) \end{aligned} \tag{50}$$

where $i = M+1, 2, \ldots, M+N_1$. For edge cracks, taking the embedded crack tip at $t = -1$, for $-1 \leqslant t \leqslant 1$, $j = M+N_1+1, M+N_1+2, \ldots, N$, we let:

$$b_{zj}(t) = g_{zj}(t)\sqrt{\frac{1-t}{1+t}} \tag{51}$$

Analogously, for an edge crack the stress intensity factor is:

$$k_{IIILi} = GG_{rz}[(r_i'(-1))^2 + (r_i(-1)\theta_i'(-1))^2]^{\frac{1}{4}}g_{zi}(-1) \tag{52}$$

where $i = M+N_1+1, M+N_1+2, \ldots, N$. The anti-plane strain components on the surface of the $i$-th defect, $i = 1, 2, \ldots, N$, Fig. 2, in terms of strain components in polar coordinates become:

$$\begin{aligned} \gamma_{tz}(r_i,\theta_i) &= \gamma_{\theta z}(r_i,\theta_i)\sin\phi_i + \gamma_{rz}(r_i,\theta_i)\cos\phi_i\\ \gamma_{nz}(r_i,\theta_i) &= \gamma_{\theta z}(r_i,\theta_i)\cos\phi_i - \gamma_{rz}(r_i,\theta_i)\sin\phi_i \end{aligned} \tag{53}$$

Substituting strain components $\gamma_{rz} = \tau_{rz}/G_{rz}$ and $\gamma_{\theta z} = \tau_{\theta z}/G_{\theta z}$ into Eq. (53) and eliminating stress components $\tau_{rz}$ and $\tau_{\theta z}$ between the resultant equations and Eq. (34) gives:

$$\begin{aligned} \gamma_{tz}(r_i,\theta_i) = &\left(\frac{\cos^2\phi_i}{G_{rz}} + \frac{\sin^2\phi_i}{G_{\theta z}}\right)\tau_{tz}(r_i,\theta_i) + \left(\frac{1}{G_{\theta z}} - \frac{1}{G_{rz}}\right)\sin\phi_i\\ &\times \cos\phi_i\tau_{nz}(r_i,\theta_i) \end{aligned} \tag{54}$$

The calculation of hoop stress on the surface of cavities is accomplished by employing the definition of a dislocation density function, i.e. $\gamma_{tz}(r_i(s),\theta_i(s)) = b_{zi}(s)$ and Eq. (54) and also using the fact that the $i$-th cavity surface is reaction free ($\tau_{nz}(r_i,\theta_i) = 0$) as follows:

$$\begin{aligned} &\tau_{tz}(r_i(s),\theta_i(s)) = \frac{G_{rz}G_{\theta z}}{G_{rz}\sin^2\phi_i(s) + G_{\theta z}\cos^2\phi_i(s)}b_{zi}(s),\\ &-1 \leqslant s \leqslant 1,\quad i = 1, 2, \ldots, M \end{aligned} \tag{55}$$

The system of Cauchy integral Eq. (37) in conjunction with Eq. (40) can be solved numerically. To this end, the original numerical procedure developed by Erdogan et al. (1973) may not be directly

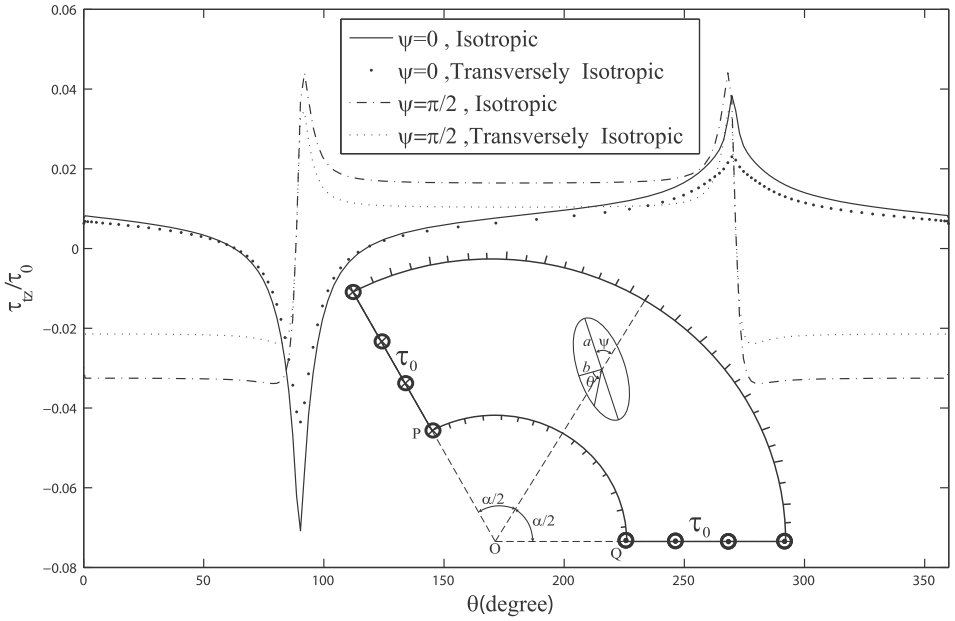


**Fig. 3.** Dimensionless hoop stress for a cavity in an isotropic/transversely isotropic sector and two different cavity orientations ($G = 1$, $G = 0.8811$).

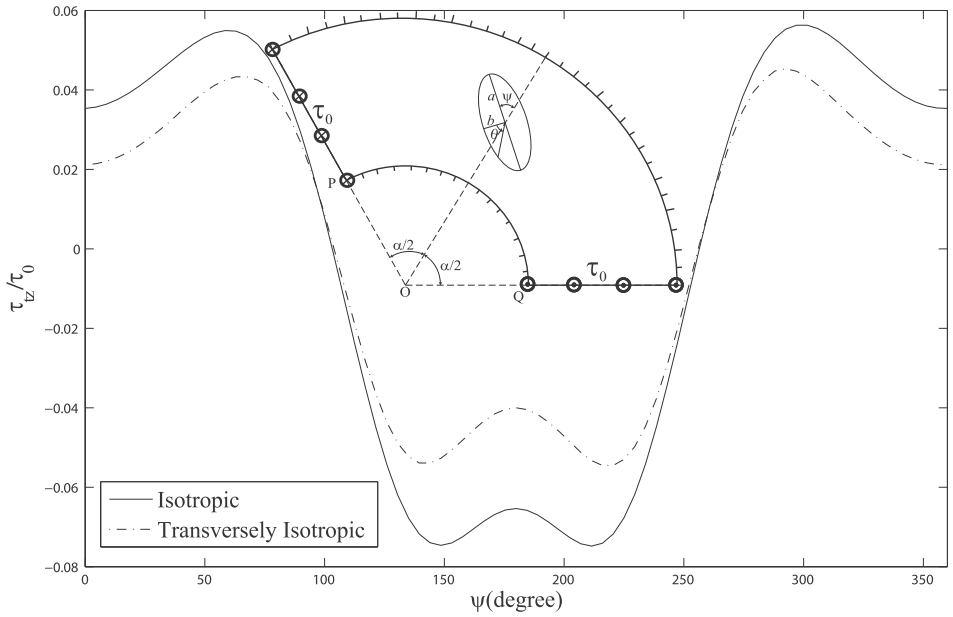


**Fig. 4.** Variation of dimensionless hoop stress for point $\theta = \frac{3\pi}{2}$ of a cavity versus the orientation angle ($G = 1$, $G = 0.8811$).

applicable since it does not consider all types of defects; i.e., embedded and edge cracks and also multiple cavities at the same time. In the study by Faal et al. (2006), a minor generalization of the numerical procedure, by means of expanding the continuous integrands of integral equations with different weight functions in terms of Tchebyshoff and Jacobi polynomials, was introduced to overcome this problem. Various weight functions resulted in various stress fields of different types of crack tips and cavity boundaries. The only approximation in the modified method was the truncating integrand infinite expansion, which would not change the accuracy of results if an adequate number of discrete points are used (Faal et al., 2006).

## 5. Numerical examples and discussions

The analysis framework developed in the preceding section allowed the consideration of a transversely isotropic sector with an arbitrary number of defects. These defects may contain embedded and edge cracks as well as cavities with different orientations. Let us consider a sector with $R_2 = 2R_1$ and a sector angle $\alpha = 2\pi/3$. In the examples to follow, the orthotropy ratio $G$ is assumed to be 0.8811 and 1.4348 for a transversely isotropic material. For the isotropic case, we have $G = 1$. The applied tractions are patch loads with the magnitude of $\tau_0$ which are distributed on the sector straight edges, except for Example 4.

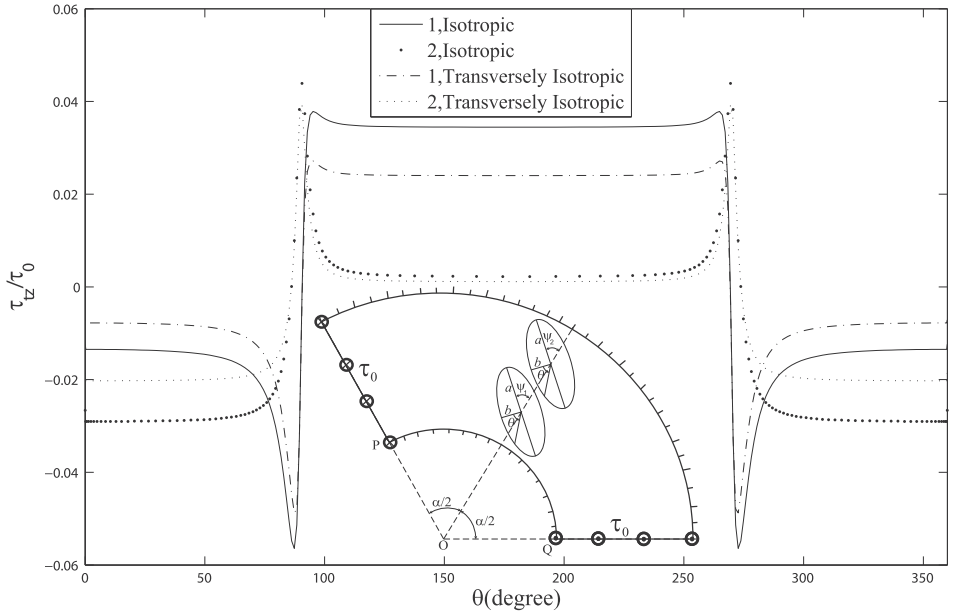


**Fig. 5.** Dimensionless hoop stress for two cavities located at the sector with two different materials (isotropic and transversely isotropic: $G = 1$ and $G = 0.8811$).

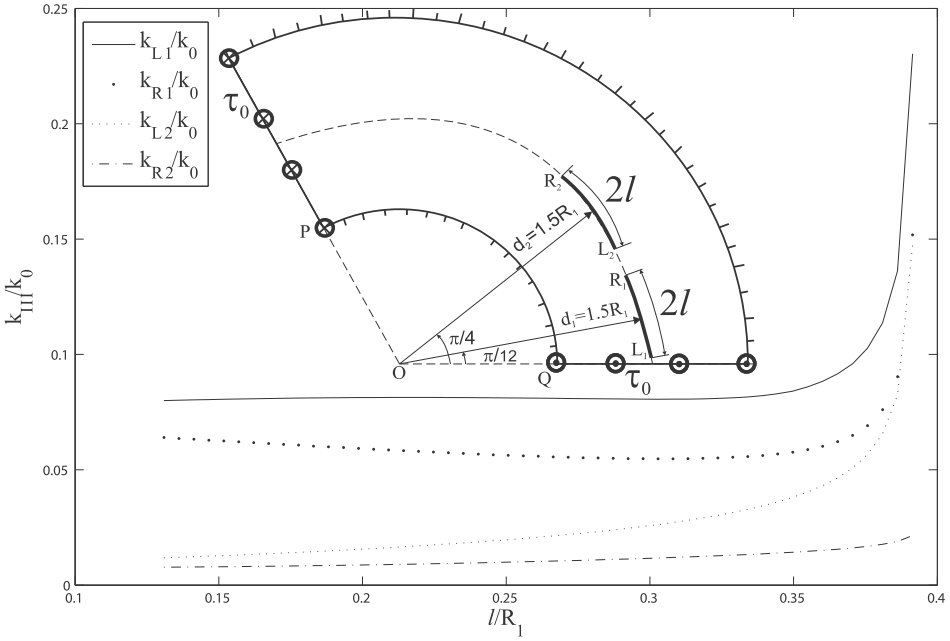


**Fig. 6.** Variation of dimensionless stress intensity factor with $l/R_1$ for an isotropic sector.

**Example 1.** Assume a transversely isotropic sector weakened by anelliptical cavity with major and minor semi-axes $a = 0.3R_1$ and $b = 0.1R_1$, respectively, as shown in Fig. 3. The center of the cavity is on the line bisecting the sector at the distance $d = 1.5R_1$. Fig. 3 depicts the dimensionless hoop stress on the surface of the cavity for two different orientations of the cavity and also different materials (isotropic/transversely isotropic ($G = 0.8811$)). The angle $\theta$ on the cavity is measured from the minor axis in the counter-clockwise direction. Based on Fig. 3, the most severe hoop stresses are observed at the sharpest points of the cavity. In the transversely isotropic sector, weaker material stiffness in the angular direction, compared to that of the radial direction, reduces the dimensionless hoop stress. For $\psi = 0$, one of the sharpest points i.e. $\theta = \frac{\pi}{2}$ is in the minimum distance of the inner sector circular edge and has the global maximum hoop stress. Also, the other sharpest point at $\theta = \frac{3\pi}{2}$ shows a local maximum hoop stress. For $\psi = \frac{\pi}{2}$, the two sharpest points of the cavity are in the identical distances of the sector bisector and have identical hoop stresses. One of the sharpest points of cavity i.e. $\theta = \frac{\pi}{2}$ for $\psi = 0$ is closer than the distance from the point $\psi = \frac{\pi}{2}$ to the fixed edge of the sector, therefore the hoop stress of point $\theta = \frac{\pi}{2}$ for $\psi = 0$ is higher than the one for $\psi = \frac{\pi}{2}$. Fig. 4 shows the variation of nondimensional hoop stress for point $\theta = \frac{3\pi}{2}$ of the cavity against the orientation angle $\psi$. Similarly, in the transversely isotropic sector, the weaker material stiffness in the angular direction compared to that of the radial direction reduces the dimensionless hoop stress. The problem is symmetric with respect to the angle $\psi = 0$ and $\psi = \pi$ as seen in Fig. 4.

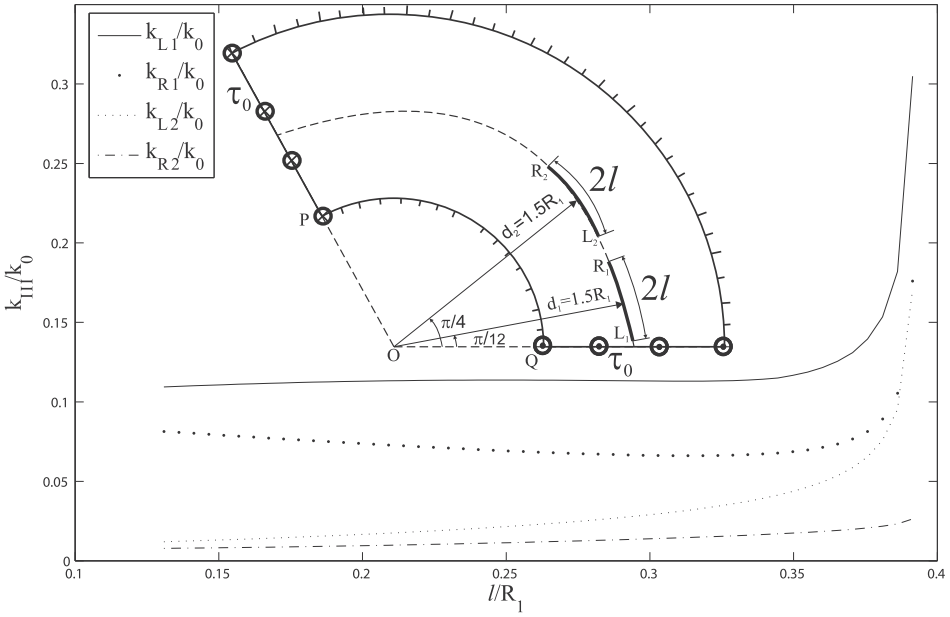


**Fig. 7.** Variation of dimensionless stress intensity factor with $l/R_1$ for a transversely isotropic sector with $G = 0.8811 < 1$.

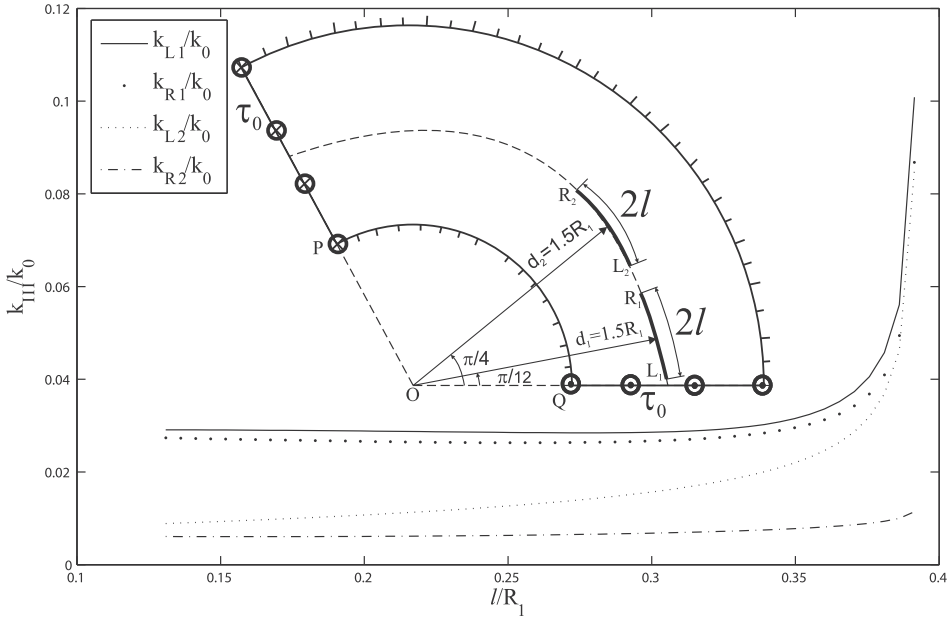


**Fig. 8.** Variation of dimensionless stress intensity factor with $l/R_1$ for a transversely isotropic sector with $G = 1.4348 > 1$.

**Example 2.** The variation of hoop stress for two identical parallel axes cavities with centers at the distances $d_1 = 1.25R_1$ and $d_2 = 1.75R_1$ from the circular edges center is shown in Fig. 5. The minor axes of the cavities are on the line bisecting the sector. Also we have $a_1 = a_2 = 0.3R_1$, $b_1 = b_2 = 0.1R_1$ and the cavities orientation angle is $\psi_1 = \psi_2 = \frac{\pi}{2}$. Similar to the example with one cavity, the most severe hoop stresses are seen at the sharpest points of cavities or points with a maximum curvature. Moreover, the stress level of the isotropic sector is higher than the sector made of the transversely isotropic material ($G = 0.8811$), mainly because the material stiffness in the angular direction is weaker than that of the radial direction.

**Example 3.** For this example let us consider two identical circular embedded cracks which are parallel with the sector circular edges. The crack centers are fixed and located at the points $(1.5R_1, \pi/12)$ and $(1.5R_1, \pi/4)$. Fig. 6 shows the variation of nondimensional stress intensity factors, $k/k_0$ at crack tips against $l/R_1$, where $l$ is the half length of embedded circular cracks and $k_0 = \tau_0\sqrt{l}$. These cracks are located at an isotropic sector. The variation of the stress intensity factor of a crack tip $R_2$ is negligible, whereas those near the crack tips $R_1$, $L_2$ and also $L_1$ increase rapidly. In particular, for the tip $L_1$, the SIF increases because of approaching the loading point. The problem was re-solved for a transversely isotropic sector with two different orthotropy ratios, $G = 0.8811$ and $G = 1.4348$,

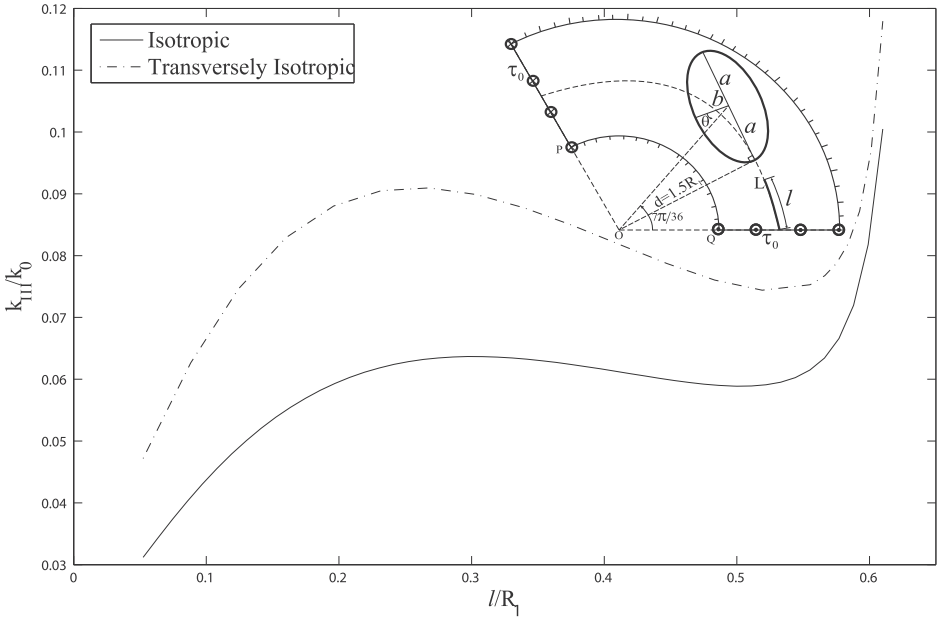


**Fig. 9.** Variation of dimensionless stress intensity factor with $l/R_1$ for edge cracking an isotropic/transversely isotropic sector with $G = 1$ and $G = 0.8811$.

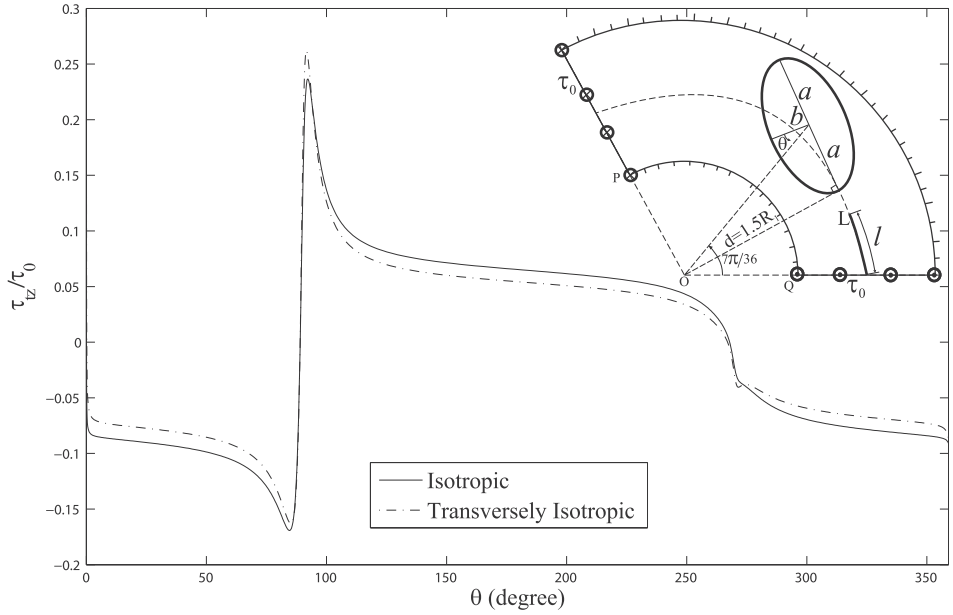


**Fig. 10.** Variation of dimensionless hoop stress for a cavity in an isotropic/transversely isotropic sector ($G = 1$ and $G = 0.8811$, $l = 0.2356R_1$).

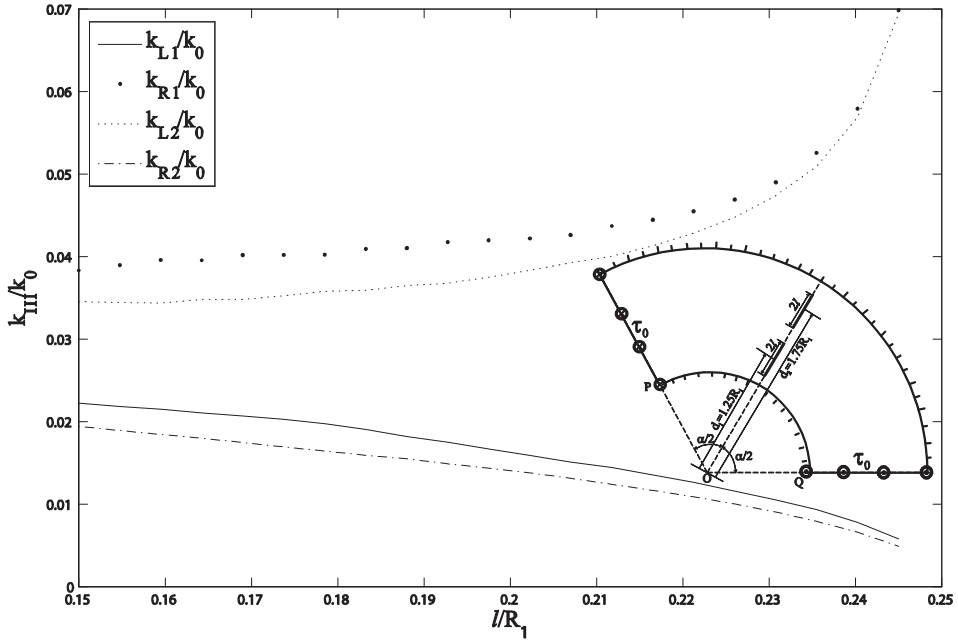


**Fig. 11.** Variation of dimensionless stress intensity factor with $l/R_1$ for an isotropic sector.

and similar trends were observed in Figs. 7 and 8, respectively. In the transversely isotropic sector ($G = 0.8811$), the weaker material stiffness in the angular direction increased the stress intensity factor. For two radial collinear cracks, one may predict that the sector's behavior would be opposite, which will be shown in Example 5. Comparison of Figs. 7 and 8 shows that increasing the orthotropy ratio from $G = 0.8811$ to $G = 1.4348$ reduces the SIF of the crack tips. Consequently, there is a logical reduction of SIF by increasing the orthotropy ratio from $G < 1$ to $G = 1$.

**Example 4.** Now we consider a sector weakened by a circular edge crack and an elliptical cavity with the length of major semi-axis $a = 0.3R_1$ and minor semi-axis $b = 0.1R_1$. The major axis of the cavity is tangent to the circle with radius $1.5R_1$ and the center of the cavity is located at the line with the angle $\theta = 7\pi/36$. The circular edge crack is parallel with the sector circular edges and in equal distances from the lower and upper boundaries. The patch loads are distributed on the sector straight edges except for the small gap with length $0.1R_1$

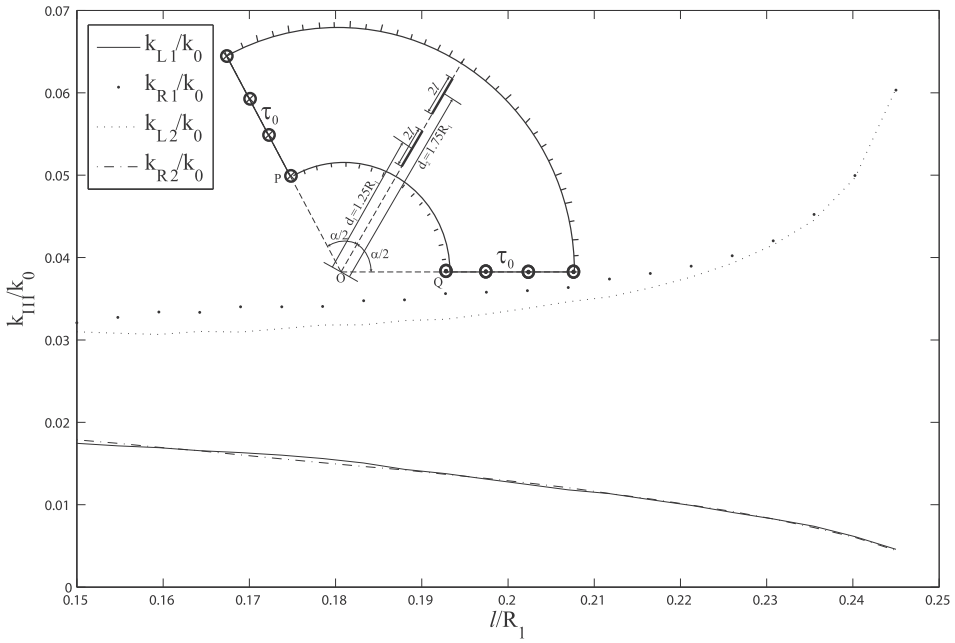


**Fig. 12.** Variation of dimensionless stress intensity factor with $l/R_1$ for a transversely isotropic sector with $G = 0.8811 < 1$.

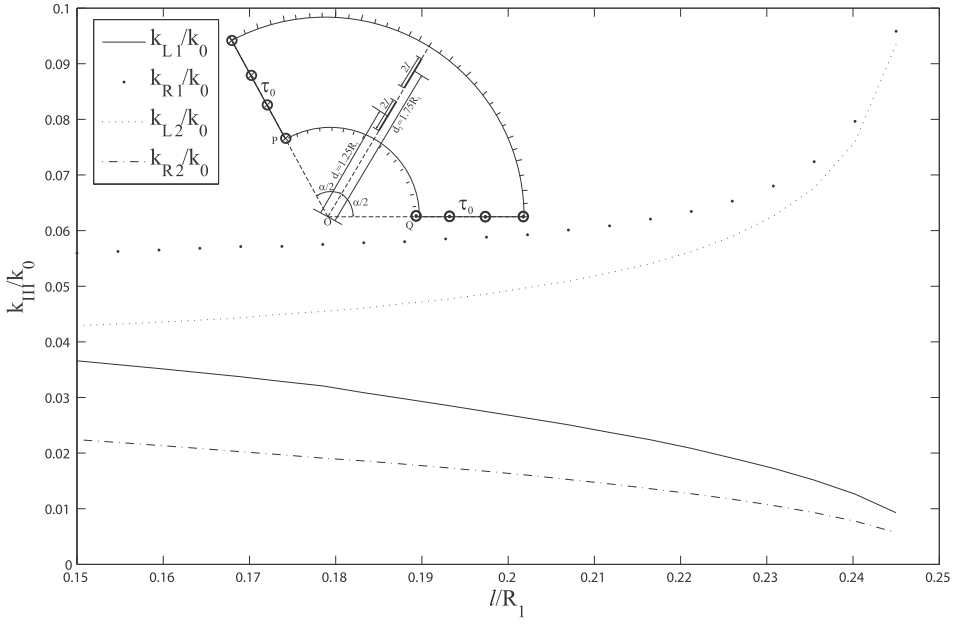


**Fig. 13.** Variation of dimensionless stress intensity factor with $l/R_1$ for a transversely isotropic sector with $G = 1.4348 > 1$.

around the starting point of the edge crack. Fig. 9 shows the dimensionless stress intensity factors, $k/k_0$, for the crack tip versus the dimensionless crack length $l/R_1$. For all crack lengths, the magnitude of SIF in the isotropic sector is higher than that of the transversely isotropic sector. As the crack tip approaches the sharpest point of the elliptical cavity, $k/k_0$ at the tip L increases rapidly. As the crack length advances, SIF increases and when the crack tip recedes from the loading point, SIF decreases. In the mid points, depending on which of the aforementioned effects becomes dominant, SIF decreases or increases. The latter cause, i.e., receding from the loading point, may explain the reason for the reduction of SIF in the middle portion of the plot in Fig. 9. Near the sharpest point of the elliptical cavity $(\theta = \frac{\pi}{2})$, where the crack tip is approached, the absolute value of the dimensionless hoop stress is maximized (Fig. 10).

**Example 5.** This example contains a sector weakened by two equally-sized radial cracks bisecting the sector angle. The distance between the centers of the cracks is $0.5R_1$ and the distance from the center circular edges to the center of the first crack is $d_1 = 1.25R_1$. Figs. 11–13 show the normalized stress intensity factors (SIF), $k/k_0$ of crack tips against $l/R_1$ where $l$ is the half length of the embedded radial cracks. As can be seen from these figures, SIF increases rapidly while the distance between the tips of cracks decreases. The formation of regions with high stress levels is attributed to the interaction of geometric singularities. Moreover, the slow reduction of other crack tips versus the crack length may be notable. Interestingly, compared to the case in Example 3, an inverse trend is seen in Example 4 where the SIF for the isotropic sector is smaller than that of the transversely isotropic sector. Similar to the previous example, the comparison of Figs. 12 and 13 shows that when the orthotropy ratio is increased, the SIF of the crack tip is amplified.

For validation purposes, for an infinite wedge ($R_1 = 0$ and $R_2 \to \infty$) weakened by two equal-sized radial cracks bisecting the apex angle, we re-examined the solution procedure. The distances between the each crack center and wedge apex are $d_1 = l/10$ and $d_2 = 3l/10$, respectively, where the applied traction is a patch load on the two wedge edges with the length $l = 0.1$ (m). The dimensionless stress intensity factors ($k/k_0$) determined by the present approach were found to be in excellent agreement with the results in Fig. 4 of Faal et al. (2004).

## 6. Concluding remarks

An analytical solution for the problem of transversely isotropic sectors weakened by Volterra-type screw dislocations was first obtained in terms of two new definite functions. Consequently, the stress field in a transversely isotropic sector under traction on its straight edge(s) was presented in a compact form, where the load and geometric singularity of stress field was shown. The dislocation density on the crack surfaces is obtainable by solving a set of integral equations of the Cauchy type singular. Finally, the distributed dislocation technique can be used to solve problems including multiple cracks and cavities with smooth geometries. The presented examples on the embedded and edge cracks, as well as cavities revealed that:

(1) The normalized stress intensity factor of the crack tips increases rapidly as they approach either each other, or near the sharp points of cavities or the loading point.
(2) The stress intensity factor at crack tips for both transversely isotropic ($G \neq 1$) and isotropic ($G = 1$) materials is symmetrically increased by an increase of the crack length. In the transversely isotropic sector ($G < 1$), however, the weaker material stiffness in the angular direction reduces the stress intensity factor for radial collinear cracks and increases for circular cracks. Increasing the orthotropy ratio showed a similar trend for the stress intensity factor.
(3) The stress intensity factor of a crack tip that is closer to the sharpest point of the elliptical cavity increases as the crack approaches the cavity boundary. Also the largest value of dimensionless hoop stress was observed at the points of the cavity boundary with minimum curvature, which are at the nearest distances from the inner sector circular edges. The latter observation is because of the presence of regions with a high stress concentration. A similar trend for the dimensionless hoop stress but with higher magnitude was noted on the cavity of the isotropic sector. Also the stress intensity factor and hoop stress for finite wedge were higher than those for a sector because of the singularity of a finite wedge apex (for some apex angles), while the sector corners are not singular.

In summary, the stress intensity factor of crack tips in transversely isotropic sectors can depend on critical factors such as the distance of the crack tip from the load, fixed edges or corners, and the curvature of cavities. As a future work, individual and combined effects of these factors on the stress intensity factor may be evaluated for different sector problems following the analytical solution procedure provided in this work. Other structural configurations and material types could also be considered, however the analytical solvability of the problem is still a limiting factor.

## Acknowledgments

Authors would like to thank the anonymous referees as well as the Editor-in-Chief, Dr. David A. Hills, for their constructive feedback and recommendations. Also the editorial assistance of Mr. Zach Barrett from the University of British Columbia-Okanagan is greatly acknowledged.

## Appendix A. Kernels of the integral equations

$$
\begin{aligned}
k_{ij}(s,t) = -\frac{\kappa G_{rz}}{4\pi r_i}\sum_{m=0}^{\infty}\Big\{\sin\phi_i\Big\{&\varphi_m(r_i/r_j,\pi(\theta_j-\theta_i)/\alpha)\\
&+\varphi_m(r_i/r_j,\pi(\theta_j+\theta_i)/\alpha)+\varphi_m\Big(r_ir_j/R_2^2,\pi(\theta_j-\theta_i)/\alpha\Big)\\
&+\varphi_m\Big(r_ir_j/R_2^2,\pi(\theta_j+\theta_i)/\alpha\Big)+\varphi_m\Big(r_jR_1^2/r_iR_2^2,\pi(\theta_j-\theta_i)/\alpha\Big)\\
&+\varphi_m\Big(r_jR_1^2/r_iR_2^2,\pi(\theta_j+\theta_i)/\alpha\Big)+\varphi_m\Big(R_1^2/r_ir_j,\pi(\theta_j-\theta_i)/\alpha\Big)\\
&+\varphi_m\Big(R_1^2/r_ir_j,\pi(\theta_j+\theta_i)/\alpha\Big)\Big\}\\
&+G\Big\{\psi_m(r_i/r_j,\pi(\theta_j+\theta_i)/\alpha)-\psi_m(r_i/r_j,\pi(\theta_j-\theta_i)/\alpha)\\
&+\psi_m\Big(r_ir_j/R_2^2,\pi(\theta_j+\theta_i)/\alpha\Big)-\psi_m\Big(r_ir_j/R_2^2,\pi(\theta_j-\theta_i)/\alpha\Big)\\
&-\psi_m\Big(r_jR_1^2/r_iR_2^2,\pi(\theta_j+\theta_i)/\alpha\Big)+\psi_m\Big(r_jR_1^2/r_iR_2^2,\pi(\theta_j-\theta_i)/\alpha\Big)\\
&-\psi_m\Big(R_1^2/r_ir_j,\pi(\theta_j+\theta_i)/\alpha\Big)\\
&+\psi_m\Big(R_1^2/r_ir_j,\pi(\theta_j-\theta_i)/\alpha\Big)\Big\}\cos\phi_i\Big\}\sqrt{(r_j')^2+\Big(r_j\theta_j'\Big)^2},\quad R_1\leqslant r_i\leqslant r_j
\end{aligned}
$$

$$
\begin{aligned}
k_{ij}(s,t) = -\frac{\kappa G_{rz}}{4\pi r_i}\sum_{m=0}^{\infty}\Big\{\sin\phi_i\Big\{&\varphi_m(r_ir_j/R_2^2,\pi(\theta_j-\theta_i)/\alpha)\\
&+\varphi_m\Big(r_ir_j/R_2^2,\pi(\theta_j+\theta_i)/\alpha\Big)+\varphi_m\Big(r_iR_1^2/r_jR_2^2,\pi(\theta_j-\theta_i)/\alpha\Big)\\
&+\varphi_m\Big(r_iR_1^2/r_jR_2^2,\pi(\theta_j+\theta_i)/\alpha\Big)+\varphi_m(r_j/r_i,\pi(\theta_j-\theta_i)/\alpha)\\
&+\varphi_m(r_j/r_i,\pi(\theta_j+\theta_i)/\alpha)+\varphi_m\Big(R_1^2/r_ir_j,\pi(\theta_j-\theta_i)/\alpha\Big)\\
&+\varphi_m\Big(R_1^2/r_ir_j,\pi(\theta_j+\theta_i)/\alpha\Big)\Big\}\\
&+G\Big\{\psi_m\Big(r_ir_j/R_2^2,\pi(\theta_j+\theta_i)/\alpha\Big)-\psi_m\Big(r_ir_j/R_2^2,\pi(\theta_j-\theta_i)/\alpha\Big)\\
&+\psi_m\Big(r_iR_1^2/r_jR_2^2,\pi(\theta_j+\theta_i)/\alpha\Big)-\psi_m\Big(r_iR_1^2/r_jR_2^2,\pi(\theta_j-\theta_i)/\alpha\Big)\\
&-\psi_m(r_j/r_i,\pi(\theta_j+\theta_i)/\alpha)+\psi_m(r_j/r_i,\pi(\theta_j-\theta_i)/\alpha)\\
&-\psi_m\Big(R_1^2/r_ir_j,\pi(\theta_j+\theta_i)/\alpha\Big)\\
&+\psi_m\Big(R_1^2/r_ir_j,\pi(\theta_j-\theta_i)/\alpha\Big)\Big\}\cos\phi_i\Big\}\sqrt{\Big(r_j'\Big)^2+\Big(r_j\theta_j'\Big)^2},\quad r_j\leqslant r_i\leqslant R_2
\end{aligned}
$$

## References


Chen, C.-H., Wang, C.-L., 2009. A solution for an isotropic sector under anti-plane shear loadings. Int. J. Solids Struct. 46, 2444–2452.

Delale, F., 1984. Stress singularities in bonded anisotropic materials. Int. J. Solids Struct. 20 (1), 31–40.

Erdogan, F., Gupta, G.D., Cook, T.S., 1973. Numerical solution of integral equations. In: Sih, G.C. (Ed.), Methods of Analysis and Solution of Crack Problems. Noordhoof, Leyden, Holland.

Faal, R.T., Fariborz, S.J., Daghyani, H.R., 2007. Stress analysis of a finite wedge weakened by cavities. Int. J. Mech. Sci. 49, 75–85.

Faal, R.T., Fotuhi, A.R., Fariborz, S.J., Daghyani, H.R., 2004. Antiplane stress analysis of an isotropic wedge with multiple cracks. Int. J. Solids Struct. 41, 4535–4550.

Faal, R.T., Fariborz, S.J., Daghyani, H.R., 2006. Antiplane deformation of orthotropic strips with multiple defects. J. Mech. Mater. Struct. 1 (7), 1097–1114.

Faal, R.T., Daliri, A.R., Fariborz, S.J., Daghyani, H.R., 2011. Anti-Plane stress analysis of orthotropic rectangular planes weakened by multiple defects. Int. J. Solids Struct. 48, 661–672.

Faal, R.T., Pasrad, A.R., in press a. Stress analysis of two kinds of dissimilar isotropic sectors. Math. Mech. Solid.

Faal, R.T., Pasrad, A.R., in press b. Anti-Plane stress analysis of dissimilar sectors with multiple defects. Appl. Math. Model. http://dx.doi:10.1016/j.apm.2012.02.017.

Hills, D.A., Kelly, P.A., Dai, D.N., Korsunsky, A.M., 1996. Solution of Crack Problems: The Distributed Dislocation Technique. Kluwer Academic Publishers, Netherlands.

Karegarnovin, M.H., Shahani, A.R., Fariborz, S.J., 1997. Analysis of an isotropic finite wedge under anti-plane deformation. Int. J. Solids Struct. 34 (1), 113–128.

Kargarnovin, M.H., Fariborz, S.J., 2000. Analysis of a dissimilar finite wedge under anti-plane deformation. Mech. Res. Comun. 27 (1), 109–116.

Korsunsky, A.M., Hills, D.A., 1996. The solution of crack problems by using distributed strain nuclei. Proc. Inst. Mech. Eng. 210, 23–31.

Lekhnitskii, S.G., 1963. Theory of Elasticity of an Anisotropic Elastic Body. Holden-Day, USA.

Liebowitz, H., 1968. Fracture Mechanics. Academic Press, New York.

Lin, R.-L., Ma, C.-C., 2004. Theoretical full-field analysis of dissimilar isotropic composite annular wedges under anti-plane deformations. Int. J. Solids Struct. 41, 6041–6080.

Mkhitaryan, S.M., Melkoumian, N., Lin, B.B., 2001. Stress-strain state of a cracked elastic wedge under anti-plane deformation with mixed boundary conditions on its faces. Int. J. Fract. 108, 291–315.

Shahani, A.R., 1999. Analysis of an anisotropic finite wedge under antiplane deformation. J. Elast. 56 (1), 17–32.

Shahani, A.R., 2003. Mode III stress intensity factors for edge-cracked circular shafts, bonded wedges, bonded half planes and DCB's. Int. J. Solids Struct. 40, 6567–6576.

Shahani, A.R., Ghadiri, M., 2010. Analysis of anisotropic sector with a radial crack under anti-plane shear loading. Int. J. Solids Struct. 47, 1030–1039.

Weertman, J., Weertman, J.R., 1992. Elementary Dislocation Theory. Oxford University Press, New York.